Vertical-Facing Loads in Steel-Reinforced Soil Walls

I. P. Damians[1]; R. J. Bathurst[2]; A. Josa[3]; A. Lloret[4]; and P. J. R. Albuquerque[5]

Abstract: The paper investigates the influence of backfill soil, foundation soil, and horizontal joint vertical compressibility on the magnitude of vertical loads developed in steel-reinforced soil concrete panel retaining walls at the end of construction. Measurements of toe loads recorded from instrumented field walls are reviewed and demonstrate that vertical toe loads can be much larger than the self-weight of the facing. In extreme cases, these loads can result in panel-to-panel contact leading to concrete spalling at the front of the wall. Vertical loads in excess of panel self-weight have been ascribed to relative movement between the backfill soil and the panels that can develop panel-soil interface shear and downdrag loads at the connections between the panels and the steel-reinforcement elements. A two-dimensional finite-element model is developed to systematically investigate the influence of backfill soil, foundation soil, bearing pad stiffness, and panel-soil interaction on vertical loads in the panel facing. The results show that an appropriately selected number and type of compressible bearing pads can be effective in reducing vertical compression loads in these structures and at the same time ensure an acceptable vertical gap between concrete panels. The parametric analyses have been restricted to a single wall height (16.7 m) and embedment depth of 1.5 m, matching a well-documented field case. However, the observations reported in the paper are applicable to other similar structures. The general numerical approach can be used by engineers to optimize the design of the bearing pads for similar steel-reinforced soil wall structures using available commercial finite-element model packages together with simple constitutive models. **DOI: 10.1061/(ASCE)GT.1943-5606.0000874.**

CE Database subject headings: Retaining structures; Reinforcing steel; Panels; Finite element method.

Author keywords: Soil retaining walls; Steel reinforcement; Vertical loads; Facing panels; Bearing pads; Finite-element modeling.

Introduction

Mechanically stabilized earth (MSE) walls constructed with steel strip or steel grid (bar mat and steel ladder) soil reinforcement elements are now a mature technology with a long history of successful performance both in the United States and worldwide. An example of a recent 46-m-high tiered steel strip–reinforced soil wall has been described by Stuedlein et al. (2010, 2012). Design methodologies for the internal and external stability of these systems can be found in national design guidance documents [AASHTO 2010; Berg et al. 2009; British Standards Institution 2010]. The majority of these structures are constructed with steel-reinforced concrete panels that are placed in a staggered pattern. The panels are placed incrementally in concert with placement and compaction of backfill soil layers and the reinforcement elements (Fig. 1). The reinforcement elements are affixed to the back of the panels at regular vertical and horizontal spacing using a pair of steel connection tabs and a bolt or similar arrangement. A key structural feature of these panel systems is the placement of compressible bearing pads at the horizontal joint between panels (Fig. 2). These pads provide a flexible joint opening that can accommodate differential settlement while at the same time allowing vertical in-plane loading to be carried through the height of the wall face to the footing at the base of the wall. If the bearing pads are too compressible and/or there are not enough pads at a horizontal joint location, then concrete-to-concrete contact can occur between panel units leading to concrete spalling (W. J. Neely, unpublished report, 2005; Neely and Tan 2010). Examples of panel spalling are illustrated in Fig. 3. The primary mechanism leading to compression of the bearing pads is downdrag force mobilized at the back of the panel units. This downdrag force occurs when the backfill soil settles more than the vertical wall facing because of compaction of the backfill soil, compression of the backfill soil under self-weight, outward movement of the wall face, and possible settlement of the foundation soil below the structure. The downdrag forces are transmitted through soil-panel interface shear and hanging-up of the backfill soil on the connections between the panel units and the reinforcement elements (Christopher et al. 1994). Fig. 4 illustrates how panel-soil interface shear and downdrag forces contribute to wall panel vertical load. Unfortunately, it is difficult to predict the magnitude of these downdrag forces within a conventional limit equilibrium-based design framework, because these loads are attributable to relative movement between the wall face and backfill soil and complex interactions at the reinforcement-panel connections as noted previously.

[1]Ph.D. Candidate, Dept. of Geotechnical Engineering and Geo-Sciences (ETCG) and Institute for Sustainability (IS.UPC), Univ. Politècnica de Catalunya-BarcelonaTech (UPC), 08034 Barcelona, Spain. E-mail: ivan.puig@upc.edu

[2]Professor, GeoEngineering Centre, Civil Engineering Dept., Royal Military College of Canada, Kingston, ON, Canada K7K 7B4 (corresponding author). E-mail: bathurst-r@rmc.ca

[3]Professor, Dept. of Geotechnical Engineering and Geo-Sciences (ETCG) and Institute for Sustainability (IS.UPC), Univ. Politècnica de Catalunya-BarcelonaTech (UPC), 08034 Barcelona, Spain. E-mail: alejandro.josa@upc.edu

[4]Professor, Dept. of Geotechnical Engineering and Geo-Sciences (ETCG), Univ. Politècnica de Catalunya-BarcelonaTech (UPC), 08034 Barcelona, Spain. E-mail: antonio.lloret@upc.edu

[5]Professor, Dept. of Geotechnics and Transportation, School of Civil Engineering, Architecture, and Urban Design, State Univ. of Campinas (Unicamp), 13083-852 Campinas, São Paulo, Brazil. E-mail: pjra@fec.unicamp.br

Note. This manuscript was submitted on April 18, 2012; approved on November 29, 2012; published online on December 1, 2012. Discussion period open until February 1, 2014; separate discussions must be submitted for individual papers. This paper is part of the ***Journal of Geotechnical and Geoenvironmental Engineering***, Vol. 139, No. 9, September 1, 2013. ©ASCE, ISSN 1090-0241/2013/9-1419–1432/$25.00.

(a)

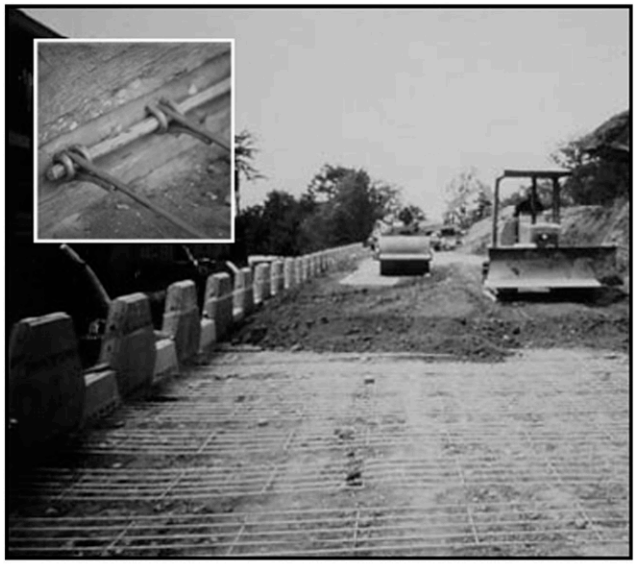

(b)

Fig. 1. Metallic reinforced soil wall systems: (a) steel strip reinforcement [image from Choufani et al. (2011); reprinted with permission from Pan-Am 64th Canadian Geotechnical Conference]; (b) bar mat reinforcement [connection details from Berg et al. (2009)]

In this paper, the authors first demonstrate that significant downdrag forces are possible in these structures based on field measurements reported in the literature. The properties of typical bearing pads are reviewed, and then, a two-dimensional (2D) finite-element model (FEM) is developed to investigate the combined influence of vertical joint compressibility, backfill soil stiffness, foundation soil compressibility, and panel-soil interface shear on vertical load through the wall face. This paper demonstrates how numerical parametric analysis can be used by design engineers to optimize the number and selection of the bearing pads to be located at the horizontal joint between concrete panels to satisfy a target compression of the bearing pads and avoid panel-to-panel contact.

Vertical Wall Loads from Monitored Structures

The internal stability design of steel-reinforced soil walls is currently based on a semiempirical approach, which has been calibrated against reinforcement loads recorded in monitored structures. Useful summaries of these monitored structures including geometry, steel reinforcement, and soil properties have been reported by Allen et al. (2001, 2004), Bathurst et al. (2008, 2009, 2011), Huang et al. (2012), and Miyata and Bathurst (2012b). These earlier papers also demonstrate that current design methods are reasonably accurate at predicting reinforcement loads under operational (working stress) conditions. However, only a few structures in these databases have included measured vertical load transmitted to the wall footing from the wall facing. Some details of these walls are summarized in Table 1. Calculated vertical loads recorded at the base of the wall facings using load cell measurements are shown in Fig. 5(a). Also shown in the figure are the vertical toe loads based on the self-weight of the facing panels. There are small differences in the slope of the self-weight plots as a result of differences in panel thickness. In all the case studies, the recorded vertical toe loads are greater than the self-weight of the facing units. It is convenient to introduce a vertical load factor defined as the ratio of total vertical load to column self-weight. For the three steel strip wall case studies, the load factor at the end of construction is in the range of 1.8–2.8 [Fig. 5(b) and Table 1]. For the steel bar mat wall, the load factor at the end of construction is 4.7. Christopher et al. (1994) mentioned that this large value is likely because of downdrag loads at the connections. Berg et al. (2009) recommend that the type and number of bearing pads be selected assuming a vertical load factor of 2–3 at the location of the horizontal joint.

It should be noted that the case studies identified in Table 1 are restricted to steel-reinforced soil walls. However, there are similar data for an instrumented full-scale 6-m-high geosynthetic-reinforced soil wall with incremental concrete panels constructed in the laboratory (Tajiri et al. 1996). The computed vertical load factor for this wall was 2.2.

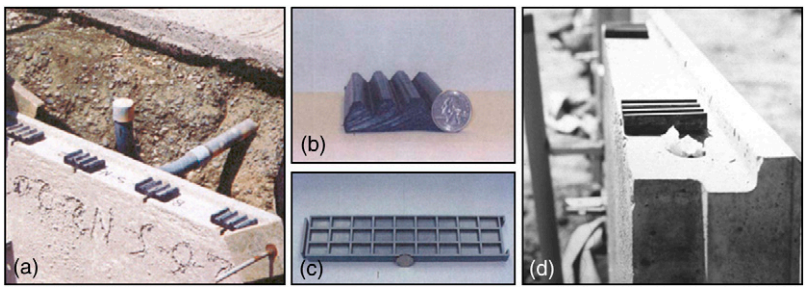

Fig. 2. Example bearing pads [(a), (b), and (c) from W. J. Neely, unpublished report, 2005; reprinted with permission from Flatiron West, Inc.; (d) from Berg et al. (2009)]

J. Geotech. Geoenviron. Eng. 2013.139:1419-1432.

(a)

(b)

Fig. 3. Spalling of concrete panel facing units: (a) panel width 1.5 m [image from Thome and Janke (2005); reprinted with permission from Deep Foundation Institute]; (b) panel width 2.25 m (image from W. J. Neely, unpublished report, 2005; reprinted with permission from Flatiron West, Inc.)

Bearing Pads

Steel-reinforced soil walls constructed with incremental concrete panels include provision for vertical deformation, differential settlement, and rotation by incorporating polymeric bearing pads placed at the horizontal joints between the concrete panels. These pads are needed to reduce downdrag forces, to prevent concrete-to-concrete panel contact, and to ensure a minimum gap between panels (Berg et al. 2009). The most common materials are ethylene propylene diene monomer (EPDM), high-density polyethylene (HDPE), and neoprene (Neely and Tan 2010). For example, the instrumented wall reported by Runser et al. (2001) used two neoprene pads per joint. However, material properties and dimensions of the pads used in their study are not reported. The mechanical stiffness of the pads used with concrete facing panels is influenced by the contact area because of cavities or grooves (voids) formed in the pads (e.g., waffle-type bearing pads). These treatments can result in a 20–30% reduction in the contact area. The nominal thickness of the pads is typically 20 mm. However, 25-mm-thick pads have also been used for high walls and for walls where large downdrag forces attributable to high backfill surface loads can be expected (Choufani et al. 2011). The enclosed plan area for individual bearing pads used in practice can vary between products. For instance, Neely and Tan (2010) gave examples of pads with perimeter plan dimensions from 0.007 (EPDM) to 0.018 m^2 (HDPE). Example vertical stress-strain curves from laboratory compression tests are shown in Fig. 6. The initial elastic modulus (E_{pad}) can be computed using the secant slope passing through the elastic strain limit and is approximately 15–75 MPa depending on the constituent material type and voids. For 20-mm-thick pads, the elastic limit corresponds to approximately 2–9 mm of compression (10–50% vertical strain). Choufani et al. (2011) reported that the wall performed well with the 25-mm-thick bearing pads compressing up to 80%. This means that the horizontal gap between panels at the end of construction was approximately 5 mm. This is the same value reported for the reference instrumented wall (Runser 1999) at the end of construction.

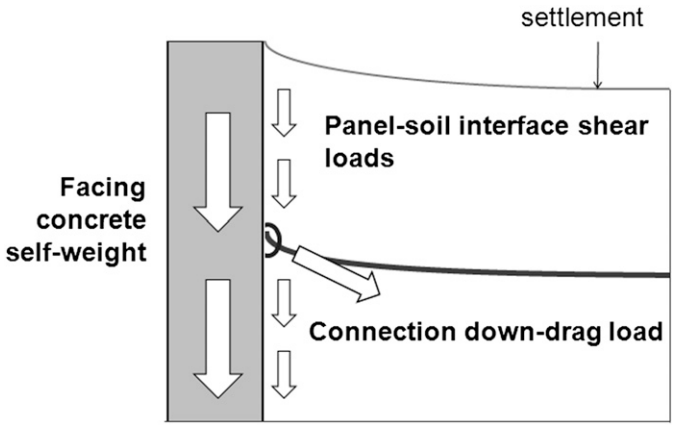

Fig. 4. Contributions to vertical axial loads in concrete facing panels

Numerical Modeling

General

Parametric analyses using a 2D FEM were carried out to investigate the influence of joint compressibility, backfill soil stiffness, foundation stiffness, and panel-soil interface shear on vertical facing panel loads. The program *PLAXIS* (2008) was used to carry out the numerical simulations. The numerical model is shown in Fig. 7. The height of the panel wall ($H = 16.7$ m) and depth of toe embedment ($D = 1.5$ m) were chosen to be close to the height of the instrumented field wall ($H = 16.9$ m) reported by Runser et al. (2001) and to match the embedment depth of this structure. The width of the numerical model was selected to concurrently optimize computation time and minimize the influence of problem boundaries. The length of the steel reinforcement elements was taken as $L = 0.7H$, which is a typical recommended minimum value in design codes (AASHTO 2010; Berg et al. 2009). The wall facing was modeled as discrete

J. Geotech. Geoenviron. Eng. 2013.139:1419-1432.

Table 1. Case Studies with Measured Vertical Footing Loads

Case study number	Reinforcement type	Wall height (m)	Soil unit weight (kN/m^3)	Soil friction angle (degrees)	Vertical load factor[a]	Reference
1	Steel strip	6.0	17.7	38	2.1	Chida and Nakagaki (1979)
2	Steel strip	10.5	16.8	36–37	2.5	Bastick et al. (1993)
3	Steel strip	16.9	20.8	38	1.8–2.8	Runser (1999), Runser et al. (2001)
4	Bar mat	6.1	20.4	35	4.7	Christopher et al. (1994)

[a]Ratio of total vertical load at base of facing panel units to self-weight of the panels.

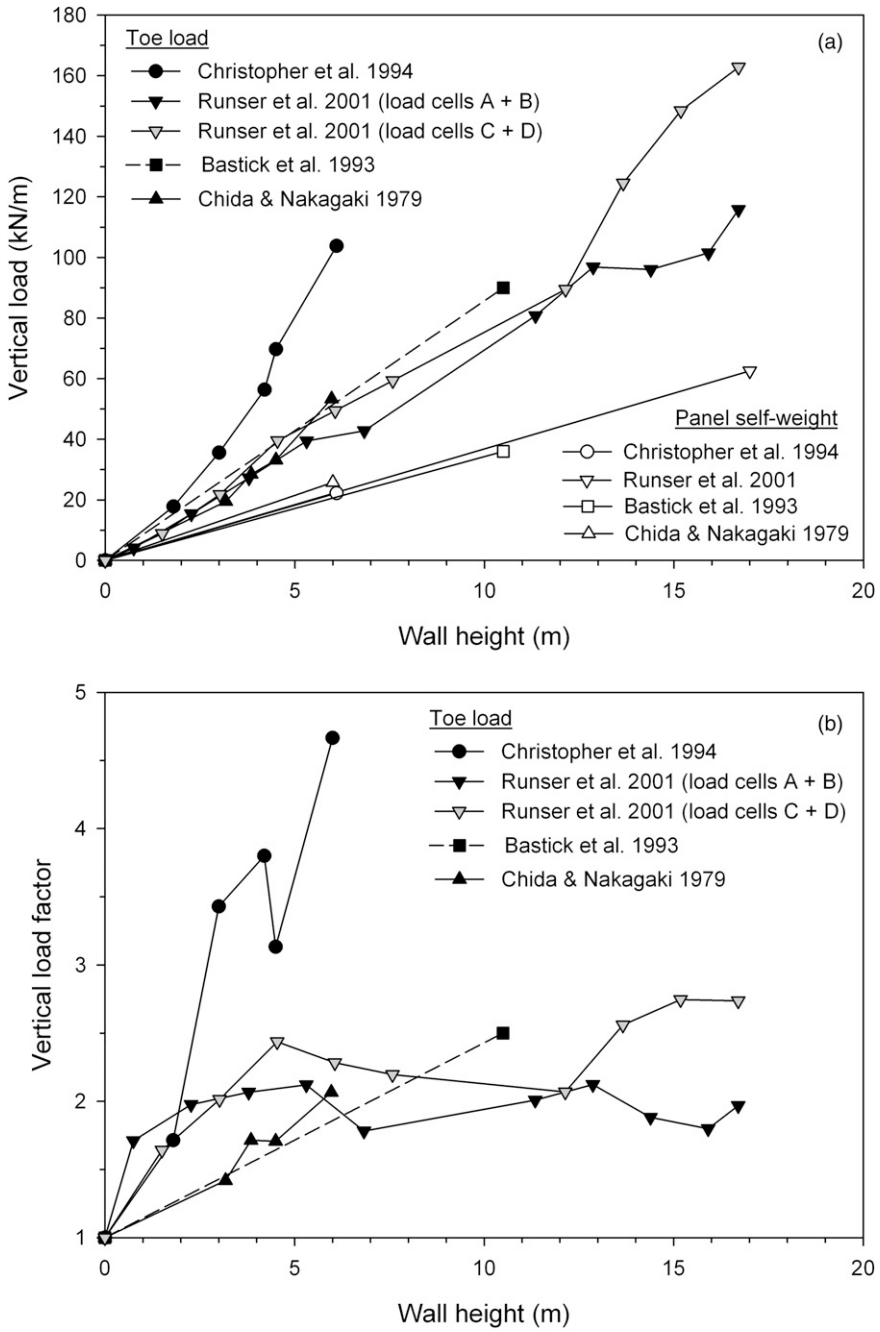

Fig. 5. Vertical toe load response from instrumented field walls: (a) measured vertical toe load versus wall height; (b) vertical load factor versus wall height where load factor is the ratio of measured vertical toe load to wall panel self-weight

J. Geotech. Geoenviron. Eng. 2013.139:1419-1432.

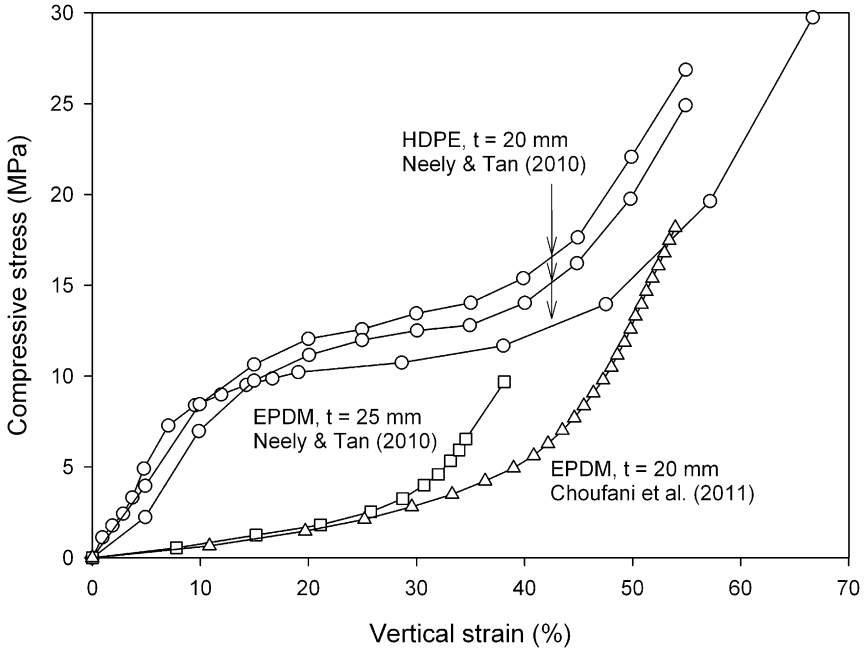

Fig. 6. Compression behavior of HDPE and EPDM bearing pad materials

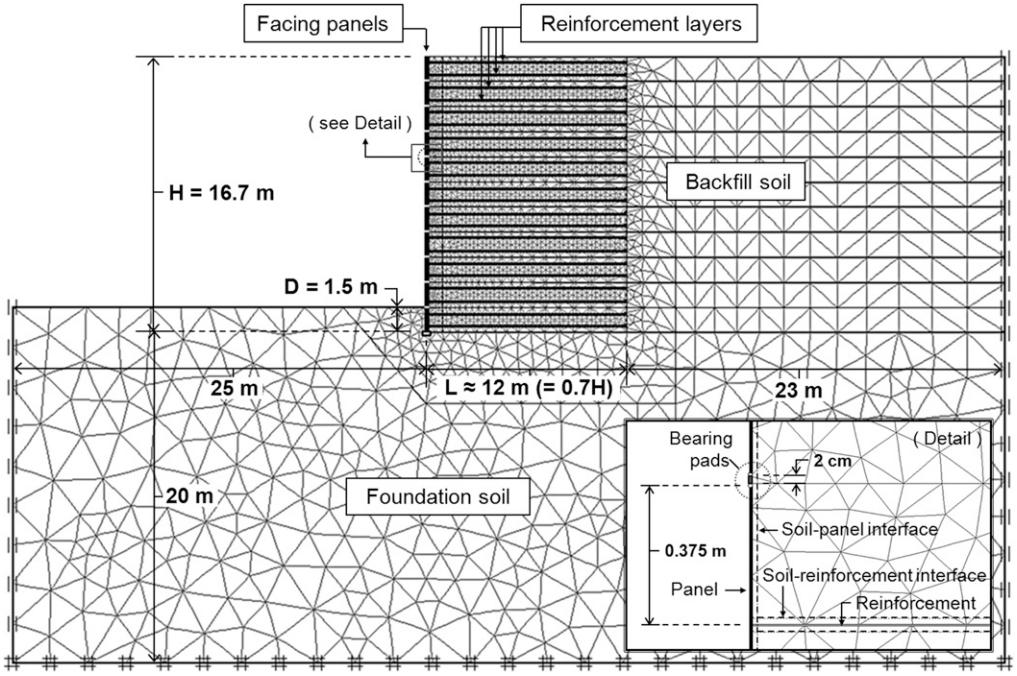

Fig. 7. Geometry of 2D FEM

panels of 1.5 m height with a horizontal joint thickness of 20 mm. The panels and joints (bearing pads) were modeled using linear-elastic beam elements. The beam elements were connected through hinge contacts with zero rotational stiffness. Hence, vertical and horizontal loads can be transmitted at the contact between each bearing pad and adjoining concrete panels but not bending moment. This approach allows for vertical compression of the panel joints (bearing pads) and rotation at each joint. Only numerical results in which there was a positive gap are presented. No attempt was made to simulate the concrete-to-concrete contact condition, which in practice should be avoided. The soil zones were modeled as elastic-plastic Mohr-Coulomb materials. Two horizontal rows of reinforcement elements were attached to each panel unit, which matches the typical arrangement for steel-reinforced soil walls (vertical spacing = 0.75 m; Runser et al. 2001). Each connection provided full rotational freedom at these locations. The facing column was seated on a concrete leveling pad that was 0.3 m wide and 0.15 m thick (Berg et al. 2009). For simplicity, the soil in front of the wall was taken as the foundation soil. The numerical wall was built incrementally from the bottom up to simulate construction in the field.

J. Geotech. Geoenviron. Eng. 2013.139:1419-1432.

Material Properties

Material properties for the concrete facing panels and horizontal joints are summarized in Table 2. The material type, dimensions, and number of bearing pads can vary between projects. The *PLAXIS* beam elements were used for the concrete panels and bearing pad joints. The equivalent axial stiffness for the joints with polymeric pads was computed as

$$(\mathrm{EA})_{\mathrm{joint}} = E_{\mathrm{pad}} A_{\mathrm{pad}} \frac{n_{\mathrm{pad}}}{L_p} \quad (1)$$

where E_{pad} = elastic modulus of the pad; A_{pad} = perimeter (enclosed) plan area of a single bearing pad; n_{pad} = number of pads per joint; and L_p is the width of the panels (minus any overlap) along the running length of the wall face. The values in Table 2 are representative for each material and most common panel width (1.5–2.5 m measured at the front face). Panel widths vary in practice depending on the type of steel-reinforced soil system. The elastic modulus (E_{pad}) for EPDM and HDPE pads was taken at 40–50% and 10–20% strain, respectively, using the data in Fig. 6. To keep the numerical modeling simple, potential strain hardening that can occur at larger compressive strains was not considered in this study. The axial stiffness values given in Table 2 represent typical minimum values for incremental concrete panel reinforced soil walls (i.e., two bearing pads per joint for the EPDM and HDPE cases). A third configuration with no polymeric pads was examined by assuming that the entire horizontal joint was concrete. In the numerical model, the same beam element representing the equivalent continuous bearing pad is used as before, but the axial stiffness of this element is assigned a very high value. This configuration allows the panels to rotate at the location of the horizontal joints as is the case for the polymeric bearing pads. Finally, it should be noted that the influence of a wide range of possible panel joint stiffnesses was examined in this investigation by considering different numbers of bearing pads and/or bearing pad elastic moduli (i.e., EPDM or HDPE). The concrete pad scenario is a hypothetical case only and is used to provide a maximum limit on joint vertical stiffness for the parametric study.

The soil zones were modeled as linear-elastic material with Mohr-Coulomb failure criterion. Material properties for the soil zones are summarized in Table 3. Five different backfill soils and two different foundation soils were considered in this investigation. The range of elastic modulus values for the backfill soil correspond to the range of elastic secant modulus values computed at 50% of the failure deviatoric stress for three different soils compacted to different densities (Boscardin et al. 1990). The range of backfill soil modulus values also matches values of silty sand to dense sand or loose gravel reported by Bowles (1996). Single elastic modulus estimates for soils are well known to be an imperfect mechanical characteristic of soil stiffness because of the sensitivity of soil stiffness to confining pressure. However, the focus of the current study is to investigate the influence of relative stiffness of the backfill and foundation soil on wall vertical face loading under working stress conditions. Hence, the Boscardin et al. (1990) data were used as a guide to select a range of compacted soil stiffness values to investigate a wide range of relative vertical loading responses. The lowest value used for the backfill soil (type 5) in this study does

Table 2. Concrete Panel and Joint Beam Properties

Material	Parameter	Values		
Concrete precast panels	Elastic modulus (GPa)	35		
	Axial stiffness, EA (GN/m)	6.0		
	Bending stiffness, EI(MN/m^2/m)	11		
	Poisson's ratio	0.15		
Bearing pads		EPDM	HDPE	Concrete[a]
	Elastic modulus, E_{pad} (MPa)[b]	15–25	45–74	~35,000
	Axial stiffness, $(\mathrm{EA})_{\mathrm{joint}}$ (MN/m)	0.13	1.1	6,000
	Bending stiffness, EI(kN/m^2/m)	0.25	2.10	11,000
	Poisson's ratio	0.5	0.4	0.15

[a]Simulates the idealized case of no polymeric bearing pads between panels.
[b]Equivalent elastic modulus (E_{pad}) based on total (perimeter) plan area of individual pads. The range of values depends on the elastic strain limit used to back-calculate the modulus in Fig. 6.

Table 3. Soil Properties

Material	Parameter		Values	
Backfill	Unit weight (kN/m^3)		19	
	Cohesion (kPa)		5[a]	
	Friction angle (degrees)		36	
	Dilatancy angle (degrees)		6	
			>1.0 m from face	<1.0 m from face
	Elastic modulus (MPa)	Soil backfill type 1	100	50
		Soil backfill type 2	70	35
		Soil backfill type 3	50	25
		Soil backfill type 4	30	15
		Soil backfill type 5	10	5
	Poisson's ratio		0.3	
Foundation	Unit weight (kN/m^3)		18	
	Cohesion (kPa)		50	
	Friction angle (degrees)		30	
	Elastic modulus (MPa)	Foundation soil type 1	1,000	
		Foundation soil type 2	10	
	Poisson's ratio		0.3	

[a]Soil assumed to be a no-tension material.

J. Geotech. Geoenviron. Eng. 2013.139:1419-1432.

not imply that poorly compacted soils (or very compressible soils) should be used in the construction of these types of structures.

The combinations of soil type shown in Table 3 allow ten different cases to be examined with respect to relative stiffness of the backfill soil and foundation stiffness. For the backfill soil zone, a column of soil 1 m wide was assumed in the numerical models to account for the reduced stiffness of the soil because of the use of lighter compaction equipment, which is recommended practice close to the facing panel (Berg et al. 2009). To keep the numerical modeling as simple as possible, no attempt was made to simulate compaction effects by applying a transient surcharge pressure at each soil layer during construction (Huang et al. 2009). Finally, it can be noted that the numerical simulation results were sensibly independent of the magnitude of the cohesive strength assigned to the soil in the numerical models. This is because the simulations were restricted to working stress conditions and not taken to soil failure.

Material properties for the reinforcement are listed in Table 4. The *PLAXIS* geogrid element was used to model the reinforcement elements as continuous sheets that have only axial stiffness and can transmit load to the surrounding soil through interface shear. The choice of the word geogrid in the *PLAXIS* program to describe this generic element type is unfortunate, because the reinforcement in the current investigation is metallic and not polymeric. The equivalent linear-elastic axial stiffness of the geogrid element for each layer of reinforcement elements is computed using Eq. (1) but with reinforcement elastic modulus, cross-sectional area, and number of reinforcement elements per panel row. For steel strips, the area is the rectangular cross section of each steel strap; for steel grid systems, this parameter is the circular cross section area of each longitudinal member. The axial stiffness values summarized in Table 4 vary with depth, because the number of steel strip elements in a row may vary with depth (Runser et al. 2001) and the cross section area of the elements may change with depth as is the case for some steel ladder walls. Both approaches are used in design practice to account for increasing horizontal earth pressure with depth below the wall crest. Finally, it can be noted that the magnitude of axial stiffness values falls within the range of values found in databases for instrumented steel strip walls and steel grid (bar mat) walls summarized by Bathurst et al. (2011) and Huang et al. (2012).

Interfaces

The *PLAXIS* interface elements were used to model strength and stiffness between soil and reinforcement elements and between the soil and concrete facing panels. These elements include an interface reduction factor (R), which is the ratio of the interface shear strength to the shear strength of the surrounding soil (called the interface friction coefficient hereafter). The reader is referred to the *PLAXIS* (2008) reference manual for further details on interface modeling. The concrete panel-soil interface was assigned a value of $R = \tan\delta/\tan\phi = 0.3$ [where ϕ is the peak friction angle of the soil (36°) and δ is the concrete soil interface friction angle (12°)] and zero dilatancy angle. The ratio of $R = 0.3$ falls between values back-calculated from horizontal loads computed using strain gauges mounted on the reinforcement layers close to the panel connections and embedded pressure cells at the back of the facing panels and from vertical loads at the base of the wall (Runser 1999; Runser et al. 2001). These values were computed at the end of construction, so it is possible that the back-calculated interface friction angle is the mobilized value and not the peak available interface friction angle. For this reason, simulations were also carried out using $R = 0.45$ and 0.6 corresponding to $\delta = 18$ and 24°, respectively. These higher values match values reported in the literature [Naval Facilities Engineering Command (NFEC) 1986]. The reinforcement elements were assumed to be perfectly bonded to the surrounding soil by assigning $R = 1$ (i.e., $\delta = \phi$). This approach is consistent with the very high pullout resistance that has been documented for steel strip and steel grid reinforcement materials (Schlosser and Elias 1978; Miyata and Bathurst 2012a; Bathurst et al. 2011). It should be noted that interface shear was also assumed to be mobilized between the front of the wall facing and the foundation soil over the embedment depth $D = 1.5$ m.

Table 4. Reinforcement Properties

Height above toe of wall (m)	Linear-elastic stiffness $(EA)_{reinf}$ (MN/m)
0–2.3	88
2.3–6.1	73
6.1–9.9	59
9.9–16	44
>16	73

Results

General

Global deformation response for combinations of backfill soil and foundation soil are illustrated in Fig. 8 for the base case of interface shear coefficient $R = 0.3$ and two HDPE bearing pads between the panel units. It should be noted that even for the largest deformation case [Fig. 8(a)] the wall remains at the working stress condition because: (1) the strains in the reinforcement layers were less than the steel yield strain; (2) shear stresses between the soil reinforcement elements and the soil were well below the interface shear strength; and (3) there were no contiguous failure surfaces in the reinforced soil zone, retained soil zone, or foundation.

The deformations in this figure are exaggerated by a factor of five to help identify differences in deformation trends and magnitudes that result from the four combinations of soil stiffness shown. For example, the largest (bulk) deformations occur for the case with both soil zones assigned (low) $E = 10$ MPa [Fig. 8(a)], and the smallest deformations occur when the highest values of E are used for both the backfill soil (100 MPa) and the foundation (1,000 MPa) [Fig. 8(d)]. As expected, the settlement at the base of the wall is proportional to and largely controlled by the stiffness of the foundation soil. For example, the settlement at the toe is approximately 300 mm for the most compressible foundation cases [Figs. 8(a and c)] and approximately 3 mm for the stiffest foundation cases [Figs. 8(b and d)]. It is interesting to note that average toe settlement for the steel-reinforced soil wall reported by Runser et al. (2001) was 32 mm. This value is close to the predicted settlement at the wall toe of 27 mm using a foundation elastic modulus of 100 MPa in the current study. This gives confidence that the range of foundation stiffness values in this numerical study captures the toe settlement in the field case study reported by Runser et al. (2001). Fig. 8(c) shows that the reinforced soil mass rotates backward when the foundation soil has 1/10 the stiffness of the backfill soil. The potential for negative rotation of a steel-reinforced soil wall mass when seated on a relatively soft (yielding) foundation has been noted by Jones and Edwards (1980).

As mentioned earlier in the paper, the focus of this parametric study is on the influence of relative soil stiffness and vertical joint stiffness on the development of vertical wall facing loads. Hence, assessment of reinforcement load predictions is not an objective. Nevertheless, it is interesting to note that the magnitude of peak

J. Geotech. Geoenviron. Eng. 2013.139:1419-1432.

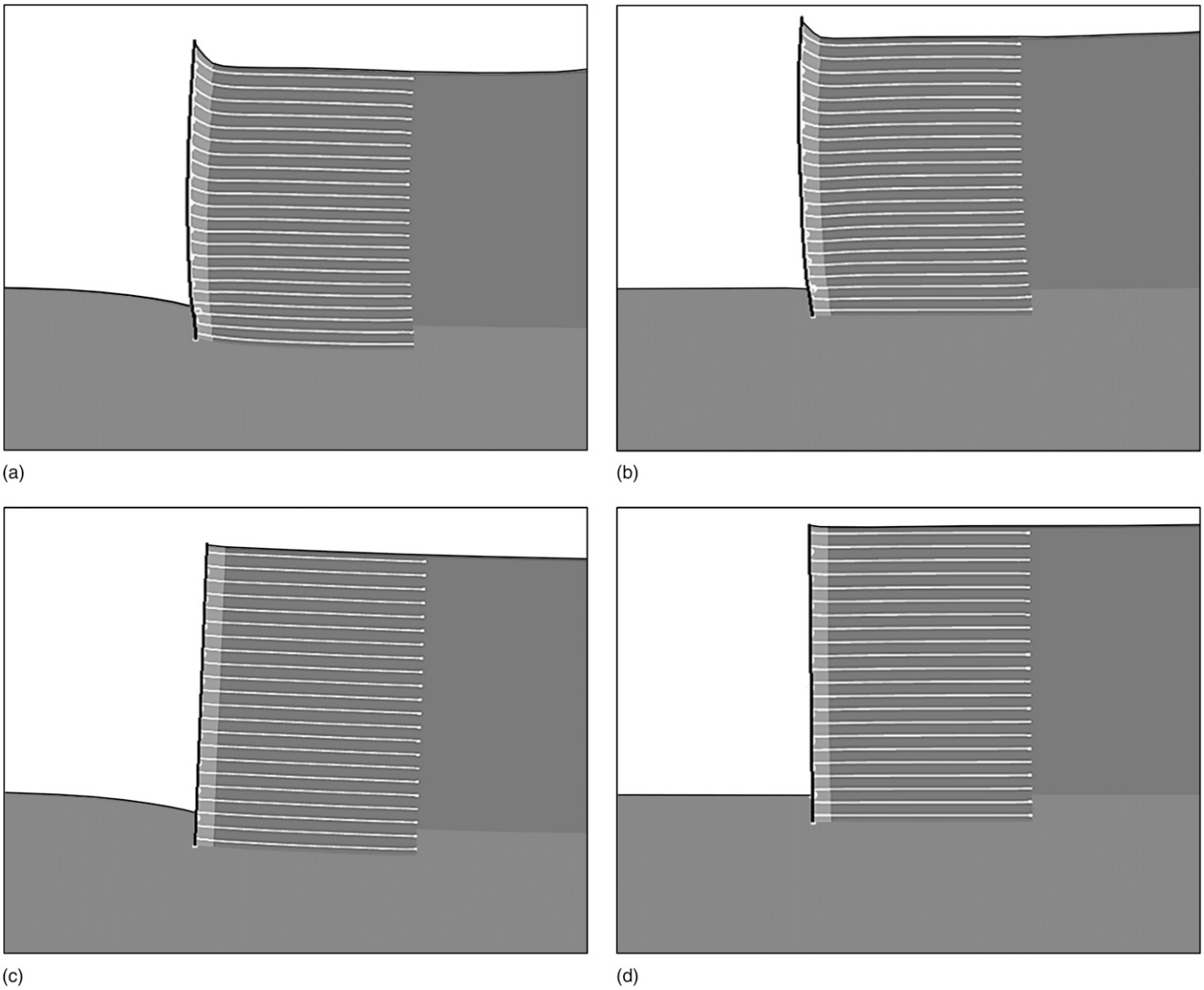

Fig. 8. Global soil wall deformations illustrating influence of relative stiffness of the backfill and foundation soils; displacements have been increased by a factor of five: (a) E(backfill) = E(foundation) = 10 MPa; (b) E(backfill) = 10 MPa, E(foundation) = 1,000 MPa; (c) E(backfill) = 100 MPa, E(foundation) = 10 MPa; (d) E(backfill) = 100 MPa, E(foundation) = 1,000 MPa

reinforcement loads generated for the case with E(backfill) = 100 MPa and E(foundation) = 10 and 1,000 MPa [Figs. 8(c and d)] was in the range of 60−65 kN/m, which is comparable to the 64 kN/m reported by Runser et al. (2001). For the same combination of soils, the magnitude of peak connection reinforcement load was in the range of 33−55 kN/m, which is comparable to the 41 kN/m reported in the same study. This gives confidence that the magnitudes of numerical results are reasonable. The range in magnitude of reinforcement loads from all simulations was not practically influenced by the type of bearing pads (and joint axial stiffness values) shown in Table 2 (i.e., within ±3% of the base case with the stiffest soils). However, for each combination of soil type with the same interface friction coefficient value there were local changes in the distribution of loads that can be ascribed to the influence of joint compressibility.

The numerical simulations were carried out to investigate wall response under operational (working stress) conditions. This criterion was satisfied by noting that all steel reinforcement strains were less than the yield strain of the steel (0.19% axial strain).

Influence of Joint Stiffness and Soil Stiffness on Vertical Facing Panel Loads

Figs. 9(a and c) provide a summary of the total vertical loads through the height of the concrete panel walls and component contributions attributable to downdrag and panel-soil interface shear for two combinations of the backfill and foundation soil. The two cases shown are the extreme combinations for foundation stiffness [i.e., E(backfill) = 100 MPa with E(foundation) = 10 and 1,000 MPa]. For both cases, the total vertical load at each panel joint location increases in the order of increasing material joint axial stiffness (i.e., EPDM, HDPE, and concrete). The contribution of the panel self-weight to the total vertical load is shown by the linearly increasing line in these two figures. The total vertical load values for all soil and panel joint stiffness cases are greater than the panel self-weight at each joint elevation and at the base of the wall because of the connection downdrag loads and mobilized panel-soil interface shear.

The total vertical loads for each case increase with depth below the wall crest until the top of the bottom embedded panel. The largest

J. Geotech. Geoenviron. Eng. 2013.139:1419-1432.

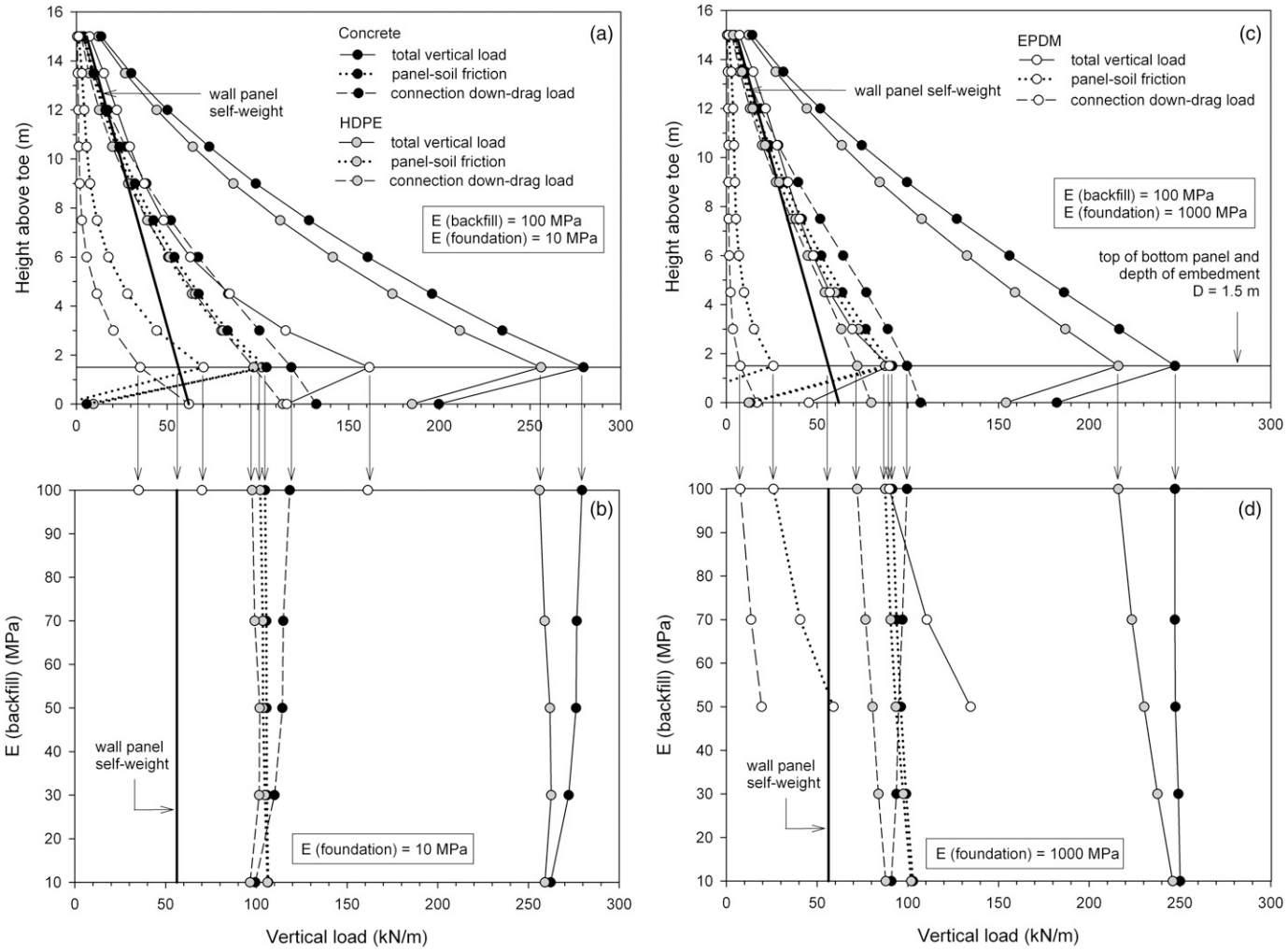

Fig. 9. Influence of joint stiffness material on total and contributing vertical facing panel loads with panel-soil interface friction coefficient $R = \tan\delta/\tan\phi = 0.3$: (a) stiff backfill soil in combination with lower stiffness foundation soil; (b) influence of backfill soil stiffness and lower stiffness foundation soil on vertical load at top of bottom panel; (c) stiff backfill soil in combination with higher stiffness foundation soil; (d) influence of backfill soil stiffness and higher stiffness foundation soil on vertical load at top of bottom panel

total vertical loads are recorded at the top of the bottom panel and then decrease to the base of the wall. This pattern is because of the development of interface shear at the front of the bottom embedded panel, which generates some vertical load capacity. In fact, for the EPDM case in Fig. 9(c), the net soil-panel friction force acts upward. This is because the panel joints are very compressible and the backfill and foundation soil are very stiff. This minimizes relative displacement between the back of the concrete panels and the backfill soil. The reinforced soil mass acts as a block with upward frictional force generated over the front embedded depth.

An important observation from Fig. 9 is that for the same bearing pad case and same backfill stiffness the total vertical load is greater for the foundation with the smaller stiffness. For example, the maximum total vertical load (top of bottom panel) for the relatively stiff foundation soil case [Fig. 9(c)] is 250, 215, and 90 kN/m for the concrete, HPDE, and EPDM cases, respectively, versus 280, 255, and 160 kN/m for the relatively compressible foundation soil case [Fig. 9(a)]. It is interesting to compare these vertical loads with values computed using classical Coulomb active earth theory for a cohesive-frictional soil in contact with a vertical wall of the same height. For the case of $R = 0.3$, the total vertical load (because of interface friction and self-weight) is about 170 kN/m. Hence, Coulomb theory underestimates the total vertical load for concrete and HDPE horizontal joint stiffness cases but overestimates the total vertical load for the relatively compressible (EPDM) horizontal joint stiffness case. These differences are expected, because (1) the walls in these simulations are assumed to be at working stress conditions (not at limit equilibrium); (2) the deformation and compressibility of the backfill and foundation soils are not considered in classical earth pressure theory; and (3) there are additional load effects attributable to reinforcement-wall connection downdrag.

Figs. 9(b and d) show the influence of backfill soil stiffness on the maximum vertical load and the contribution of downdrag and interface shear components on loads predicted at the critical panel location (i.e., top of bottom embedded panel). For the case of the most compressible joint material (two EPDM bearing pads), there is a trend of increasing load values with decreasing backfill soil stiffness. However, the data plots in these two figures for this case are truncated corresponding to numerical outcomes indicating panel-to-panel contact. For the relatively stiffer concrete and HDPE joint material cases, the influence of backfill soil stiffness is relatively little.

Fig. 10 shows the fraction of total vertical load attributable to panel self-weight, connection downdrag, and concrete panel-soil interface

J. Geotech. Geoenviron. Eng. 2013.139:1419-1432.

shear force at the top of the bottom panel as a function of the panel-soil interface shear coefficient for walls with E(backfill) = 100 MPa. For the most compressible joint case [Fig. 10(a)] and the stiffest foundation soil, the increasing fraction of toe load is in the order of downdrag load, panel-soil friction, and panel self-weight (open symbols). For the matching conditions but with the most compressible foundation soil case, the increasing fraction of toe load is in the order of downdrag load, panel self-weight, and panel-soil friction (solid symbols). The influence of the panel-soil interface shear magnitude on relative load contributions is negligible. For the same cases but a stiffer HDPE joint material [Fig. 10(b)], the relative contribution of panel-soil friction increases with increasing panel-soil friction coefficient. However, the relative contributions to total vertical load are judged to be negligible based on foundation stiffness. (Compare solid and open symbol pairs.)

Fig. 11 examines the influence of panel-soil interface friction on the total load developed at the top of the bottom panel. For the relatively stiff concrete and HDPE joint cases, the total vertical load increases with increasing interface friction angle (i.e., increasing friction coefficient R). This trend is expected from classical notions of rigid wall-soil interaction. Rowe and Ho (1997) showed a similar trend of increasing vertical facing load with increasing interface friction angle from results of 2D FEM simulations of continuous panel walls but reinforced with more extensible geosynthetic reinforcement layers. However, in this study, this trend decreases with decreasing stiffness of the panel joint material and in fact is slightly reversed for the weakest (EPDM) case. A qualitative explanation is

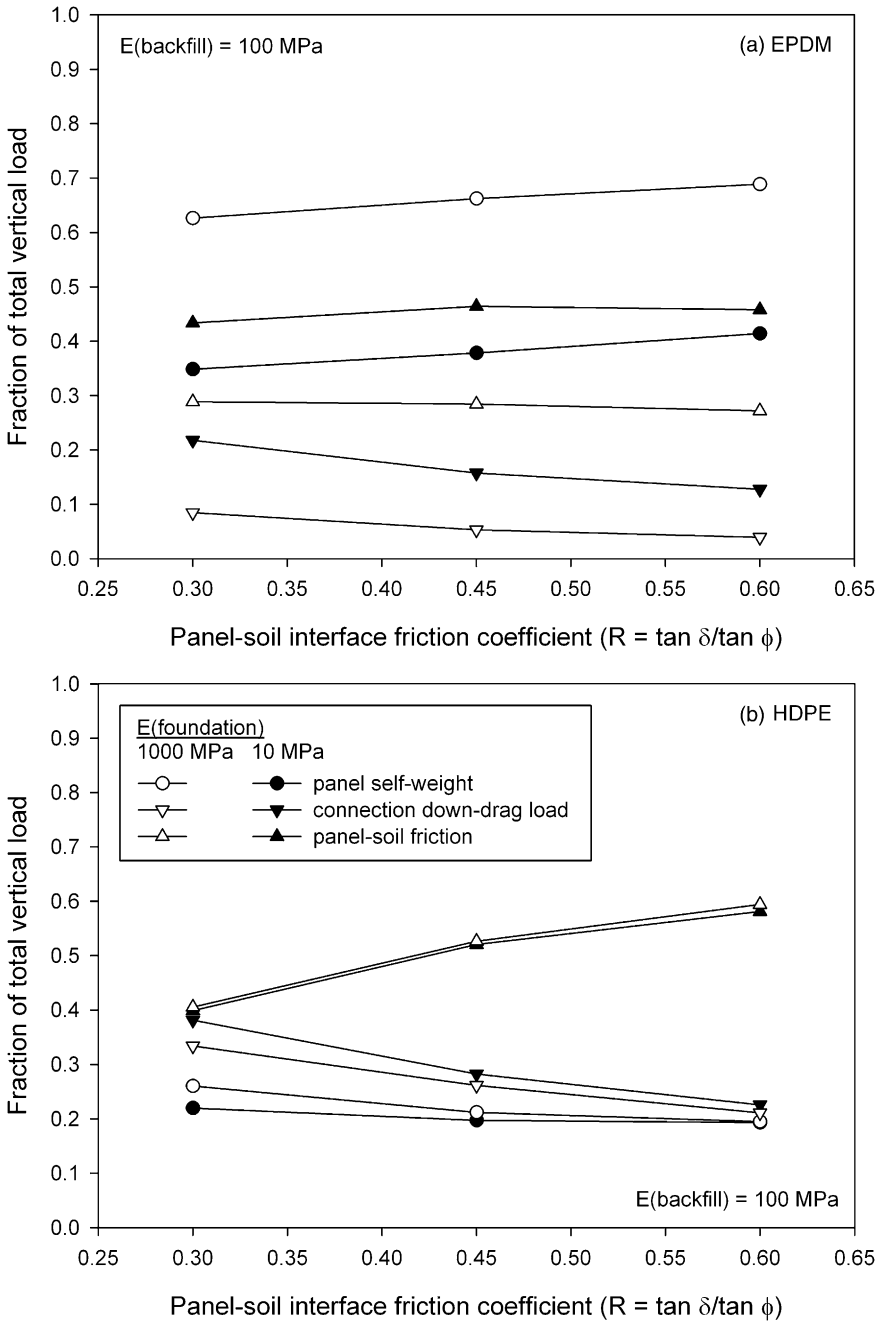

Fig. 10. Fraction of total vertical panel base load versus panel-soil friction coefficient (R)

J. Geotech. Geoenviron. Eng. 2013.139:1419-1432.

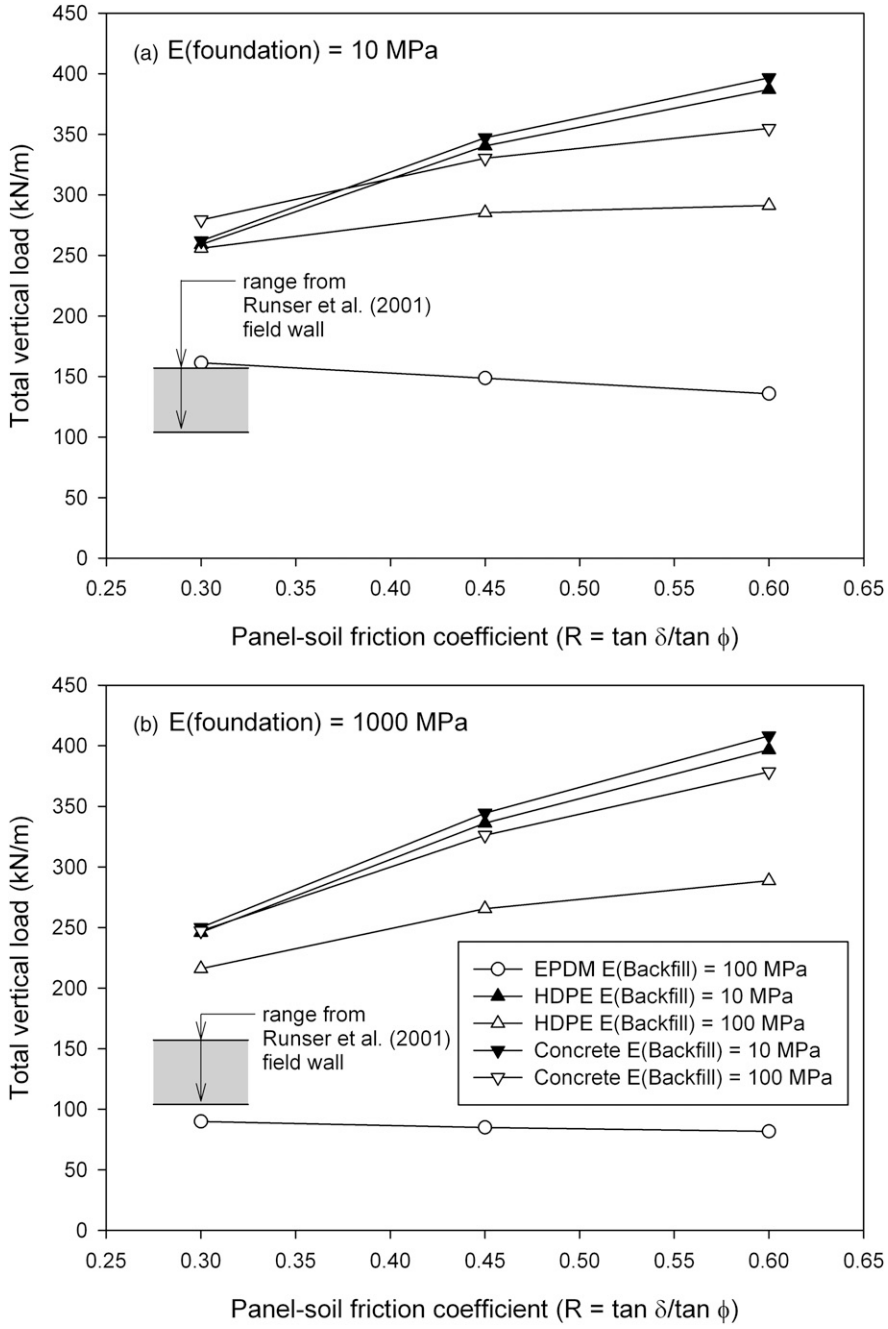

Fig. 11. Influence of panel-soil friction coefficient (R) on total vertical load at top of bottom panel; EPDM with backfill soil $E = 10$ MPa not included, because panel contact occurred

that the wall vertical stiffness for the EPDM cases is similar to the equivalent vertical stiffness of the soil behind the wall. Superimposed on the plots is the range of total vertical toe loads for the 16.7-m-high steel strip–reinforced soil wall reported by Runser et al. (2001). The range of toe loads falls between the cases for two HDPE and two EPDM bearing pads and the stiffest foundation soil case in this study [E(foundation) = 1,000 MPa; Fig. 11(b)]. In fact, the measured range of toe loads is in agreement with an interpolated value of foundation stiffness of 100 MPa between the two figures and assuming two EPDM bearing pads.

Fig. 12 shows the maximum compressive strain and gap size at the critical panel joint location as a function of the axial stiffness of the joint for the 16.7-m-high wall that is the base case in the current study. As expected, joint compressive strains decrease with increasing joint axial stiffness (EA). However, the practical influence of the magnitude of the backfill soil stiffness and foundation stiffness also decreases with increasing joint stiffness. Hence, the choice of joint stiffness in steel-reinforced soil walls becomes more important as the backfill soil stiffness decreases relative to foundation soil stiffness and/or as the foundation stiffness decreases. Examples of the type and number of 20-mm-thick bearing pads to match the joint axial stiffness values on the horizontal axis are shown in the figure. The data show that it is possible to select a sufficient number of EPDM bearing pads to keep the vertical gap between panel units to less than 5 mm for the range of soil stiffness values investigated.

J. Geotech. Geoenviron. Eng. 2013.139:1419-1432.

Fig. 13 shows the computed maximum vertical load factor for all combinations of input parameters in the current investigation and $R = 0.3$ and 0.6. The vertical load factor has been computed at the critical joint elevation, which is at the top of the bottom panel. The independent parameter in this figure is the joint axial stiffness (Table 2) normalized against the product of the backfill elastic modulus and thickness of the uncompressed joint (i.e., $t = 0.02$ m). Only data points corresponding to positive gap values are plotted. The data plots show that above a ratio of one the load factor approaches a value of 4–5 for cases with $R = 0.3$. Below this value, the load factor decreases rapidly with decreasing log value of the normalized joint stiffness. For numerical simulation results using $R = 0.6$ (i.e., large mobilized panel-soil interface shear resistance), the load factors approach a value of 6–7 beyond a normalized joint stiffness of about 10. The numerical data and field data show that compressible joint materials can be effective in reducing vertical compression loads in these structures.

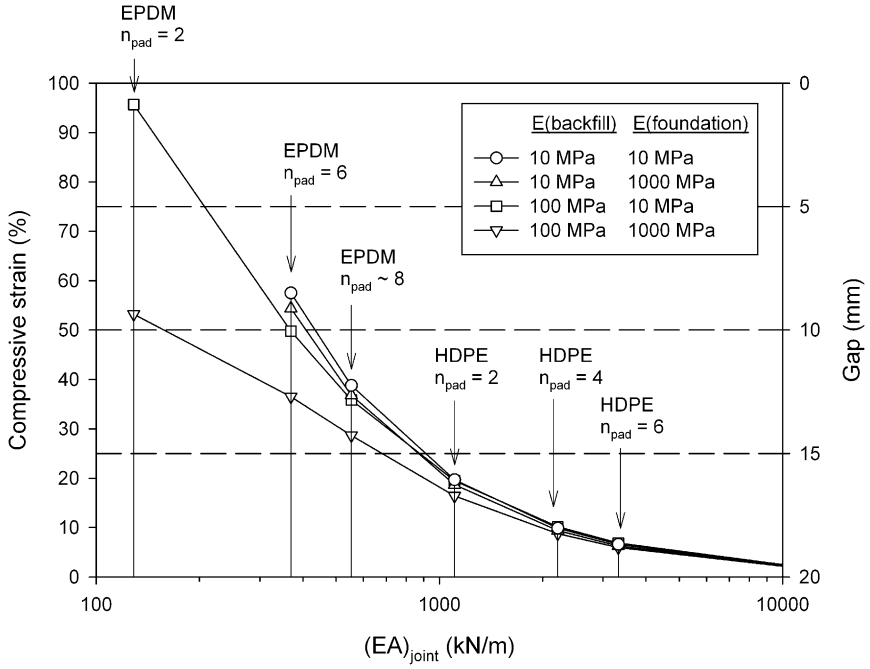

Fig. 12. Computed axial strains and joint gap thickness at top of bottom panel at end of wall construction using bearing pads with initial thickness of 20 mm; panel-soil interface friction coefficient $R = \tan\delta/\tan\phi = 0.3$

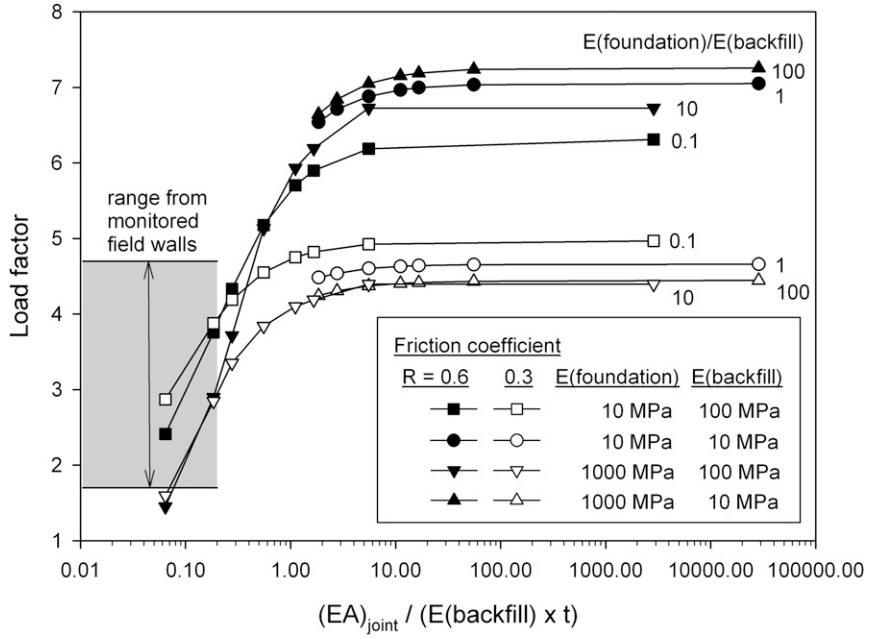

Fig. 13. Influence of relative soil stiffness and ratio of joint stiffness to local backfill stiffness on maximum vertical facing load factor; $R = \tan\delta/\tan\phi$

J. Geotech. Geoenviron. Eng. 2013.139:1419-1432.

Discussion

The investigation described in this paper is focused on steel-reinforced soil wall systems with precast concrete panels. The numerical simulations are limited to a single wall height and embedment depth. For simplicity, the analyses in this investigation have used a linear-elastic constitutive model for the soil together with a Mohr-Coulomb failure criterion. Design engineers routinely use simple constitutive models in practice even for substantial reinforced steel wall structures (Lindquist 2008).

In this investigation, the loads in the reinforcement and shear stresses in the reinforced soil zone are consistent with working stress conditions. Despite the simplicity of the soil model, the measured reinforcement loads at the end of construction are in the range recorded for an instrumented field wall of similar dimensions reported in the literature (Runser et al. 2001). More importantly, the magnitudes of predicted total vertical load include the range reported by Runser et al., and the vertical load factors reported in the current study are in the range reported for instrumented steel strip walls.

More complex constitutive soil models are available in the literature, but these models require input properties that are seldom available to design engineers. Furthermore, improved accuracy of numerical predictions using more advanced models may not be assured (Ling 2003). In practical terms, numerical models need only be as accurate as the measurements against which the predictions can be compared. As an example, Huang et al. (2009) demonstrated this point when they compared numerical predictions for a steel wire mesh–reinforced soil wall against measured values for reinforcement strains and toe loads. In one simulation, they used a linear-elastic Mohr-Coulomb soil model and in the second a more sophisticated single hardening model (Lade 2005). At the end of construction (working stress conditions), there was no practical difference between computed toe loads or reinforcement loads using the simpler soil model and the range of measured values.

Conclusions

The numerical investigation in this paper has used the example of a 16.7-m-high steel-reinforced soil wall constructed with a range of reinforced backfill soil, foundation soil, and horizontal joint stiffness to examine the development of vertical facing load at the end of construction. The following major conclusions can be made:

1. Vertical toe loads are greater than panel self-weight because of shear forces mobilized between the back of the concrete panels and the backfill soil and downdrag forces generated at the connections between the steel reinforcement elements and the concrete facing panels;
2. The magnitude of the vertical load at the bottom of the facing panels cannot be predicted accurately using conventional limit-equilibrium models because of the complex effects of deformation and compressibility of the backfill and foundation soils, horizontal joint stiffness, and additional load because of reinforcement-wall connection downdrag;
3. Numerical results show that when the backfill soil is relatively soft, the compressibility of the horizontal joint has relatively little influence on the vertical load factor (where the vertical load factor is the ratio of the total vertical load in the panel wall divided by the self-weight of the panel wall); and
4. The paper shows that an appropriately selected number and type of compressible bearing pads can be effective in reducing vertical compression loads in these structures and at the same time ensure an acceptable vertical gap between concrete panels.

Although this study has been limited to a single wall geometry and range of soil properties, the general conclusions are expected to apply to other steel-reinforced soil wall geometries. An important contribution of this study is that it provides a strategy for design engineers to investigate the influence of soil stiffness and panel joint stiffness using available commercial FEM packages together with simple constitutive models. This approach allows the engineer to optimize the selection of bearing pads for similar steel-reinforced soil wall structures.

Acknowledgments

The authors acknowledge the support of the Universitat Politècnica de Catalunya-BarcelonaTech (UPC) and the funding received through the research project BIA2010-20789-C04-01 from the Ministry of Education and Innovation of Spain. This funding allowed the first author to spend six months at the GeoEngineering Centre at Queen's-RMC during which time the research work reported in this paper was performed. Finally, the authors are grateful to David Runser, who clarified a number of details regarding the reference wall case used in this study.

References

AASHTO. (2010). *LRFD bridge design specifications*, 5th Ed., Washington, DC.

Allen, T., Christopher, B., Elias, V., and DeMaggio, J. (2001). "Development of the Simplified Method for internal stability." *Rep. WA-RD 513*, Washington State Department of Transportation, Olympia, WA.

Allen, T. M., Bathurst, R. J., Holtz, R. D., Lee, W. F., and Walters, D. L. (2004). "A new working stress method for prediction of loads in steel reinforced soil walls." *J. Geotech. Geoenviron. Eng.*, 130(11), 1109–1120.

Bastick, M., Schlosser, F., Segrestin, P., Amar, S., and Canepa, Y. (1993). "Experimental reinforced earth structure of Bourron Marlotte: Slender wall and abutment test." *Reinforcement des sols: Experimentations en vraie grandeur des annees 80*, Presses de L'École Nationale des Ponts et Chaussees, Paris, 201–228.

Bathurst, R. J., Huang, B., and Allen, T. M. (2011). "Load and resistance factor design (LRFD) calibration for steel grid reinforced soil walls." *Georisk*, 5(3-4), 218–228.

Bathurst, R. J., Nernheim, A., and Allen, T. M. (2008). "Comparison of measured and predicted loads using the Coherent Gravity Method for steel soil walls." *Ground Improv.*, 161(3), 113–120.

Bathurst, R. J., Nernheim, A., and Allen, T. M. (2009). "Predicted loads in steel reinforced soil walls using the AASHTO Simplified Method." *J. Geotech. Geoenviron. Eng.*, 135(2), 177–184.

Berg, R. R., Christopher, B. R., and Samtani, N. C. (2009). *Design and construction of mechanically stabilized earth walls and reinforced soil slopes*, Vol. I, National Highway Institute, Federal Highway Administration, U.S. Department of Transportation, Washington, DC.

Boscardin, M. D., Selig, E. T., Lin, R. S., and Yang, G. R. (1990). "Hyperbolic parameters for compacted soils." *J. Geotech. Engrg.*, 116(1), 88–104.

Bowles, J. E. (1996). *Foundation analysis and design*, 5th Ed., McGraw Hill, New York.

British Standards Institution. (2010). "Code of practice for strengthened/reinforced soil and other fills." *BS 8006*, Milton Keynes, U.K.

Chida, S., and Nakagaki, M. (1979). "Test and experiment on a full-scale model of reinforced earth wall." *Proc., Int. Conf. on Soil Reinforcement*, Vol. 2, Paris, 533–538.

Choufani, C., Wu, P., Gagnon, G., and Macintosh, M. (2011). "A precast faced mechanical stabilized earth solution for a 20 metre high mining crusher wall with various technical and site challenges." *Proc., 2011 Pan-Am Canadian Geotechnical Conf.* (CD-ROM), Canadian Geotechnical Society, Richmond, BC, Canada, 625.

Christopher, B. R., Bonczkiewicz, C., and Holtz, R. D. (1994). "Design, construction and monitoring of full scale test of reinforced soil walls and

J. Geotech. Geoenviron. Eng. 2013.139:1419-1432.

slopes." *Recent case histories of permanent geosynthetic-reinforced soil retaining walls*, F. Tatsuoka and D. Leshchinsky, eds., Balkema, Rotterdam, Netherlands, 45–60.
Huang, B., Bathurst, R. J., and Allen, T. M. (2012). "Load and resistance factor design (LRFD) calibration for steel strip reinforced soil walls." *J. Geotech. Geoenviron. Eng.*, 138(8), 922–933.
Huang, B., Bathurst, R. J., and Hatami, K. (2009). "Numerical study of reinforced soil segmental walls using three different constitutive soil models." *J. Geotech. Geoenviron. Eng.*, 135(10), 1486–1498.
Jones, C. J. F. P., and Edwards, L. W. (1980). "Reinforced earth structures situated on soft foundations." *Geotechnique*, 30(2), 207–213.
Lade, P. V. (2005). "Overview of constitutive models for soils." *Soil constitutive models: Evaluation, selection and calibration*, J. A. Yamamuro and V. N. Kaliakin, eds., ASCE, Reston, VA, 1–34.
Lindquist, D. D. (2008). "Seismic modeling of a 135-foot-tall MSE wall." *Geotechnical earthquake engineering and soil dynamics IV*, ASCE, Reston, VA.
Ling, H. I. (2003). "Finite element applications to reinforced soil retaining walls—Simplistic versus sophisticated analyses." *Proc., Geomechanics: Testing, Modeling, and Simulation, 1st Japan-U.S. Workshop on Testing, Modeling, and Simulation*, J. A. Yamamuro and J. Koseki, eds., ASCE, Reston, VA, 77–94.
Miyata, Y., and Bathurst, R. J. (2012a). "Analysis and calibration of default steel strip pullout models used in Japan." *Soils Found.*, 52(3), 481–497.
Miyata, Y., and Bathurst, R. J. (2012b). "Measured and predicted loads in steel strip reinforced c-ϕ soil walls in Japan." *Soils Found.*, 52(1), 1–17.
Naval Facilities Engineering Command (NFEC). (1986). *Design manual 7.02. Foundations and earth structures*, Alexandria, VA.
Neely, W. J., and Tan, S. L. (2010). "Effects of second order design factors on the behaviour of MSE walls." *Proc., Earth Retention Conf. 3*, ASCE, Reston, VA, 522–530.
PLAXIS. (2008). *Reference manual, 2D—version 9.0*, PLAXIS, Delft Univ. of Technology, Delft, Netherlands.
PLAXIS 9.02 [Computer software]. Delft, Netherlands, PLAXIS.
Rowe, K. R., and Ho, S. K. (1997). "Continuous panel reinforced soil walls on rigid foundations." *J. Geotech. Geoenviron. Eng.*, 123(10), 912–920.
Runser, D. J. (1999). "Instrumentation and experimental evaluation of a 17 m tall reinforced earth retaining wall." M.S. thesis, School of Civil Engineering, Purdue Univ., West Lafayette, IN.
Runser, D. J., Fox, P. J., and Bourdeau, P. L. (2001). "Field performance of a 17 m-high reinforced soil retaining wall." *Geosynth. Int.*, 8(5), 367–391.
Schlosser, F., and Elias, V. (1978). "Friction in reinforced earth." *Proc., ASCE Symp. on Earth Reinforcement*, ASCE, New York, 735–763.
Stuedlein, A. W., Allen, T. M., Holtz, R. D., and Christopher, B. R. (2012). "Assessment of reinforcement strains in very tall mechanically stabilized earth walls." *J. Geotech. Geoenviron. Eng.*, 138(3), 345–356.
Stuedlein, A. W., Bailey, M. J., Lindquist, D. D., Sankey, J., and Neely, W. J. (2010). "Design and performance of a 46-m-high MSE wall." *J. Geotech. Geoenviron. Eng.*, 136(6), 786–796.
Tajiri, N., Sasaki, H., Nishimura, J., Ochiai, Y., and Dobashi, K. (1996). "Full-scale failure experiments of geotextile-reinforced soil walls with different facings." *Proc., IS-Kyushu 96, 3rd Int. Symp. on Earth Reinforcement*, A. A. Balkema, Rotterdam, Netherlands, 525–530.
Thome, D. A., and Janke, R. C. (2005). "Rehabilitation of an existing mechanically stabilized earth wall using soil nails." *Proc., 30th Annual Conf. on Deep Foundations*, Deep Foundations Institute, Hawthorne, NJ, 1280, 49–54.

J. Geotech. Geoenviron. Eng. 2013.139:1419-1432.